Top Catal (2017) 60:1082–1093
DOI 10.1007/s11244-017-0792-2

ORIGINAL PAPER

Influence of a Zeolite-Based Cascade Layer on Fischer–Tropsch Fuels Production over Silicon Carbide Supported Cobalt Catalyst

A. R. de la Osa[1] · A. Romero[1] · J. Díez-Ramírez[1] · J. L. Valverde[1] · P. Sánchez[1]

Published online: 19 April 2017

Abstract In this work, selective production of middle distillate from synthesis gas was conducted over a cascade catalytic system in a single unit. Co/β-SiC was chosen as an efficient Fischer–Tropsch synthesis (FTS) catalyst (first layer) while proton-type H-ZSM-5 and H-βeta zeolites (second layer) were tested for the subsequent hydroprocessing to produce middle distillate from waxes. Moreover, in order to compare, a prior FTS reference experiment was performed. Catalytic materials were characterized by means of Atomic Absorption, Thermogravimetric analysis, X-Ray diffraction, N_2 adsorption–desorption, Temperature-Programmed Reduction and Temperature-Programmed Desorption. From catalytic results, a distinguishable enhancement of commercial fuels products was observed under the proposed cascade operation compared to the stand-alone configuration or physical mixture. Regardless the zeolite type, FTS over Co/β-SiC with subsequent upgrading was demonstrated to result in the complete elimination of waxes, solving the main weakness of a conventional fixed-bed reactor. Moreover, apart from a selective production of gasoline, the proposed concept provided a significant enhancement of both kerosene and diesel yields, particularly when zeolite H-βeta is incorporated to the cascade system due to its mild acidity and larger pore size.

Keywords Fischer–Tropsch · Middle distillates · Cascade · Cobalt/β-silicon carbide · Zeolite

✉ A. R. de la Osa
AnaRaquel.Osa@uclm.es

[1] Chemical Engineering Department, Faculty of Chemical Sciences and Technology, University of Castilla-La Mancha, Avda. Camilo José Cela 12, 13071 Ciudad Real, Spain

1 Introduction

From the 1980s, concern about global warming and climate change have pushed the necessity to reduce the emissions of gases responsible for the Greenhouse effect, mainly CO_2, which is produced by the use of fossil fuels. However, it is well known that the vast world energy demand comes from fossil fuels use with oil, coal and natural gas each accounting for around one quarter of global energy needs by 2040. Moreover, the depletion of fossil reserves, the increase of energy demand and environmental concerns incentive the development of technologies based on the conversion of available feedstocks into non-petroleum derived fuels.

Synthetic fuels from Fischer–Tropsch synthesis (FTS) are considered an ideal choice to replace crude oil-distillates since significantly lower emissions of hydrocarbons, CO, NO_x, particulates, sulfur and aromatics compounds are produced and also due to the possible integration of the process into power plants. Even more, defined as sustainable and renewable as can be produced from any carbonaceous resource, these synthetic fuels have gained attention worldwide as shown by different projects in Europe, Asia, North America or Australia [1].

However, FTS process generates a wide hydrocarbon spectra imposed by Anderson–Schulz–Flory distribution [2]. Therefore, additional downstream upgrading and separation steps are required to improve selectivity toward commercial middle distillates [3]. Therefore, important research has been conducted to intensify the overall sustainability and profit of the process in terms of both catalyst and reactor engineering. In this sense, the integration of both FTS process and hydrocracking in a single unit is still a challenge due to some incompatibilities of either catalyst or process conditions across the two steps [4]. To approach this integration, along with an efficient FTS catalyst, three

different strategies have been attempted: (i) physical mixture or layering of FTS and hydrocracking catalysts [5], the latter usually composed by a noble metal supported on an acid zeolite; (ii) encapsulating FT function with a hydrocracking catalyst layer [6] and (iii) dispersion of FT function on a hydrocracking catalyst support [7]. Increased selectivities to gasoline-range hydrocarbons have been successfully demonstrated but the question remains whether further improvements can also extent diesel production along with the complete elimination of waxes.

Among the potential FTS catalysts, only Co and Fe are economically feasible at industrial scale to convert synthesis gas into long-chain hydrocarbons. However, cobalt is considered the most favorable metal to that end due to its high activity and selectivity to linear paraffins and also to its low water–gas shift (WGS) activity. Particularly, Co/β-SiC has been demonstrated to be a promising FTS catalyst due to the intrinsic thermal conductivity, chemical inertness and the significant improvement of reaction performance when β-SiC is present in the catalyst formulation compared to conventional supports [8–14].

As aforementioned, it has been reported that the selective production of hydrocarbons from syngas can be attained by modification of the reaction system in terms of the first strategy. It is based on the use of the as so-called hybrid catalyst systems (a FTS catalyst together with an acid zeolite with/without noble metal doping) [15–17] either disposed in a physical mixture form [5] or involving upgrading step in a dual-three-bed reactor system [18]. Hence, in an effort to improve process performance and cost-effectiveness, the aim of this work was to study the possible integration of both FTS and hydrocracking [19] in a single unit through a cascade system composed by the promising Co/β-SiC catalyst [10, 20] and a subsequent layer of zeolite. In order to analyze differences derived from the nature of zeolite, H-ZSM-5 and H-βeta, with different physicochemical properties, were tested to convert long chain hydrocarbons into valuable fuels.

2 Experimental

2.1 Synthesis of Catalyst and Pretreatment of Hydrocracking Materials

Catalyst Co/β-SiC containing 14 wt% cobalt was prepared by successive vacuum-assisted impregnations of extrudates (1 mm diameter and length) of medium specific surface β-SiC material (SICAT Catalyst) with a cobalt nitrate (Merck, KGaA, Darmstadt, Germany) solution. The support was firstly outgassed at ambient temperature for 2 h in order to remove water and other surface impurities. A solution of the salt precursor in ethanol was then poured over the support and vacuum-outgassed at 90 °C for 2 h. After the first impregnation step the as-prepared precursor was dried at 120 °C overnight in a 240099 SELECTA oven, and calcined in a 224129 SELECTA muffle furnace (static air atmosphere, 5 °C/min heating rate) at 550 °C for 6 h in order to decompose cobalt nitrate into Co_3O_4. Note that several subsequent impregnations and heat-treatments were required to obtain the final catalyst with the specified cobalt loading. Its physicochemical properties are listed in Table 1.

Catalytic materials tested in the hydrocracking of FT waxes comprised classical microporous crystalline zeolites (i.e. ZSM-5 and βeta purchased from Zeolyst International). Prior to FTS tests, commercial zeolites were calcined at 550 °C for 3 h [21, 22] in the SELECTA muffle furnace used for catalyst preparation, thus producing the H^+-type zeolites. Their characteristics are also summarized in Table 1.

2.2 Characterization

The total amount of cobalt into the catalyst was quantified (±1% error) by atomic absorption (AA), using a SPECTRAA 220FS analyzer (Varian Australia Pty Ltd., Mulgrave, Victoria, Australia).

Surface area and porosity properties were analyzed in a Micromeritics ASAP 2010 sorptometer apparatus (Micromeritics, Norcross, GA, USA) in case of catalyst Co/β-SiC, and in a Quantachrome Quadrasorb 3SI apparatus(Quantachrome Europe) for zeolite samples, with N_2 (at −196 °C) as sorbate. Prior to analysis, samples were degassed at 180 °C (6.6×10^{-9} bar) for 16 h (Co/β-SiC) and at 300 °C (1×10^{-2} torr) for 12 h (zeolites), respectively. Total specific surface areas, mesopores size distribution and microporosity in zeolites were determined by the multi-point BET [23], Barret–Joyner–Halenda (BJH) [24] and Horwath-Kawazoe [25] methods, respectively.

X-ray diffraction patterns were collected by a Philips model X'Pert MPD with Co-filtered Cu Kα radiation (λ = 1.54056 Å) (Philips, Eindhoven, the Netherlands). XRD diffractograms were recorded over a 2θ range of 3°–90° at a 0.04° step using a 0.4 s acquisition time per step. In case of catalyst Co/β-SiC average crystallite size of Co_3O_4 was calculated at 2θ: 36.9° according to Scherrer's equation [26, 27].

TPR, NH_3-TPD and O_2 pulses measurements were all carried out with ±2% average error in an Autochem HP 2950 analyzer (Micromeritics, Norcross, GA, USA). Each sample sample (0.1 g) was firstly degassed in an argon or helium flow (by heating at 10 °C min^{-1}). In case of Temperature Programmed Reduction analysis, after degassing, temperature and detector signal were continuously recorded while heating (at 5 °C·min^{-1} heating rate) from room

Table 1 Physico-chemical properties of catalytic materials and β-SiC support

β-SiC support								
BET specific surface area ($m^2 g^{-1}$)		Pore diameter (nm)				Pore volume ($cm^3 g^{-1}$)		
27.4		9.0				0.12		
Catalyst Co/β-SiC								
Co (wt%)	Particle size (nm)		Dispersion (%)	Extent of reduction (%)	BET specific surface area ($m^2 g^{-1}$)	Pore diameter (nm)	Total pore volume ($cm^3 g^{-1}$)	
	dCo_3O_4 (2θ: 36.9°)	dCo^0						
13.0	61.5	46.1	2.1	77.8	22.0	8.3	0.09	
Zeolites								
	BET specific surface area ($m^2 g^{-1}$)			Pore volume ($cm^3 g^{-1}$)				
	Total	Micropore	Mesopore	Total	Micropore	Mesopore		
H-ZSM-5	375.2	190.1	185.1	0.37	0.08	0.29		
H-βeta	528.7	216.2	312.4	0.81	0.13	0.62		

temperature up to 900 °C under a reducing atmosphere (17 v/v % H_2/Ar). The extent of reduction was determined by pulse oxidation with O_2 of reduced samples. After reduction under pure H_2 flow at 550 °C for 5h (5°C min^{-1} heating rate), the sample was cooled to 400 °C in He and kept at this temperature for 1 h. Once any chemisorbed H_2 was desorbed, calibrated pulses of O_2 were injected into the He flow until no oxygen consumption was detected by the thermal conductivity detector. The extent of reduction calculation was based on the stoichiometric re-oxidation of Co^0 to Co_3O_4 [28, 29]. Information about the acidity of the zeolites was determined by ammonia Temperature Programmed Desorption analysis. Once the sample was outgassed (550 °C for 15 min) under He flow, ammonia was fed at 100 °C (a rate of 30 ml min^{-1}) until saturation. After NH_3 adsorption, the sample was flushed at 100 °C with He for 1 h and followed by lowering the temperature to 50 °C until TCD signal was constant. Once any physically adsorbed NH_3 was removed TPD profile was recorded by ramping the temperature from 50 to 600 °C (5 °C min^{-1} heating rate).

Thermogravimetric analysis (TG) of β-SiC support was carried out using a Mettler Toledo TGA/DSC 1 STARe SYSTEM apparatus (Mettler-Toledo AG, Schwerzenbach, Switzerland) (experimental error of ±0.5% in the weight loss measurement and ±2° in the temperature measurement). Approximately 10 mg of sample were placed in an Al_2O_3 ceramic crucible. TG curves were recorded in flowing air in the range from room temperature to 950 °C (heating rate 5 °C min^{-1}).

2.3 Activity Test

Fischer–Tropsch synthesis was tested in a MICROACTIVITY (PID ENG&TECH, Spain, MAP2GL2M4 model) facility at 2 MPa in the limits of the low reaction temperature range (220 and 250 °C). Reaction took place for 60 h time on stream (TOS) in a stainless steel down flow fixed-bed reactor (9 mm i.d. × 305 mm length) under two different configurations as illustrated in Fig. 1:

a. Conventional stand-alone fixed-bed, where catalyst (reference FTS Co/β-SiC or hybrid one) was loaded into the reactor and packed among layers of α-SiC inert material to avoid the formation of hot spots in the catalyst. The hybrid catalyst consisted of a physical mixture of 2 g of FTS catalyst with 1 g of zeolite. Note that in case of the reference experiment (in absence of zeolite) the FTS catalyst was diluted with a higher amount of α-SiC in order to balance space velocity.
b. Cascade (dual) catalyst bed: a first layer of catalyst (2 g of Co/β-SiC diluted in α-SiC + quartz wool) was followed by a second fixed-bed composed by zeolite

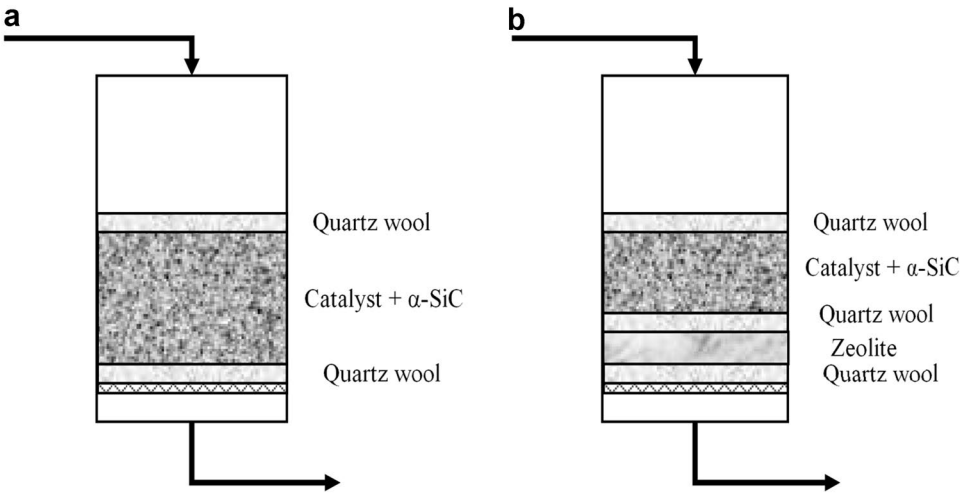

Fig. 1 Experimental catalytic **a** stand-alone; **b** cascade configurations

ZSM-5 or βeta (1 g + quartz wool). It is denoted as 'Co/β-SiC//H-zeolite'.

Prior to each Fischer–Tropsch synthesis run, the catalyst was pretreated under atmospheric pressure by reduction with pure H_2 flow (100 ml min^{-1}) at 550 °C (5 °C min^{-1} heating rate) for 5 h. After activation, the sample was pressurized up to 20 bar with N_2 flow (100 Nml min^{-1}) and set to 220 or 250 °C. Then, syngas ($CO/H_2/N_2$:3/6/1 vol ratio) was introduced to the reactor with a constant gas hourly space velocity (GHSV) of 3000 Nml g^{-1} h^{-1}. Both effluent gas compositions before and after reaction were analyzed online every 10 min by a CP-4900 Varian MicroGC. Liquid products were collected and separated in two traps of different temperatures. In addition, an extraction with *n*-hexane was required in order to separate organic (C_7–C_{20}) from aqueous phase. Then, liquid hydrocarbon products distribution (C_5^+) was analyzed offline by capillary GC (VARIAN 430) equipped with a FID detector. Each run was repeated at least three times and the selectivity in terms of CH_4, CO_2, C_2H_6, C_3H_8 and C_5^+ formation was calculated by the equations given in previous works [10, 20].

3 Results and Discussion

In an effort to improve process performance and cost-effectiveness, the goal of the present work was to study the possible integration in one-step of both FTS and hydrocracking [19] through a cascade system composed by the promising Co/β-SiC catalyst [10, 20] and a layer of zeolite under two different configurations. In order to analyze differences derived from the nature of zeolite, ZSM-5 and βeta (with different physicochemical properties) were tested to convert long chain hydrocarbons into valuable fuels.

3.1 Characterization of Catalytic Materials

Since the objective of the present investigation is to maximize the production of middle distillates, two acid zeolites (H-ZSM-5 and H-βeta) were tested in the hydrocracking of FT waxes fraction obtain from FTS over Co/β-SiC. Table 1 lists the most important textural characteristics of both zeolitic materials and β-SiC support.

The chemical composition of the prepared FTS catalyst is shown in Table 1. Data results from AA elemental analysis shows that the experimentally determined cobalt content clearly fit with the nominated one.

Regarding β-SiC support, its oxidation behaviour was studied under air atmosphere at high temperature (up to 950 °C) by means of TG-DTG analysis. Figure 2 shows that the sample was stable up to 500–550 °C. At this temperature, a slight weight loss associated with the removal

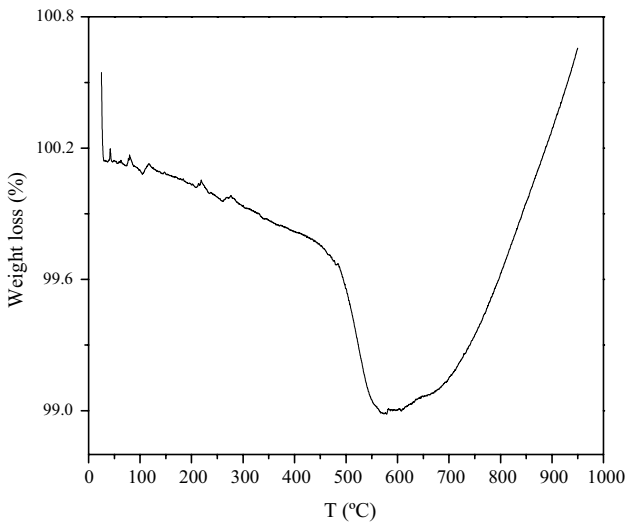

Fig. 2 TG analysis in air. **a** Co/β-SiC; **b** β-SiC

of free carbon compounds was noted [30]. From 550 to 950 °C, an increase in weight was observed, which was related to the formation of SiO_2 [31], which was similar to that reported for SiO_2–SiC-based supported catalysts.

XRD patterns of the calcined catalytic materials are illustrated in Fig. 3. It can be observed that patterns of catalyst Co/β-SiC and support shown in Fig. 3.a only displays diffraction peaks corresponding to crystalline SiC and Co_3O_4 phase. β-SiC support presented characteristic reflections of its two polytypes, which is consistent with those reported elsewhere [32]: peaks at 2θ 33.7°, 35.5° corresponds to hexagonal α-SiC (1 1 1) and (0001) while 2θ: 41.4°, 59.9° and 71.7° are related to (0 0 2), (2 0 2) and (1 1 3) face-centered cubic β-SiC, respectively [32, 33]. FTS Co/β-SiC catalyst showed the representative reflection peak at 2θ = 36.8°, from which average Co_3O_4 particle size deduced by the Scherrer equation was calculated to be 61.5 nm. Metallic cobalt particle size was calculated assuming spherical crystallites according to the following formula: $dCo\ (nm) = d(Co_3O_4) \times 0.75$ [34]. It should be noted that as reported in Table 1, its value was larger than that of the support pore size, therefore, deposition of large cobalt crystallites on the outer surface of β-SiC support may be considered.

From XRD patterns represented in Fig. 3b, c it can be seen that the proton-type ZSM-5 and βeta zeolites were highly crystalline. Reflections corresponding to zeolite H-ZSM-5 matched the typical diffraction pattern of MFI structure [35], whereas a characteristic BEA structure type was related to zeolite βeta [36].

N_2 adsorption–desorption isotherms associated to catalytic materials as well as surface area, total pore volume and pore size data are summarized in Fig. 4 and Table 1. In agreement with literature on β-SiC cobalt supported catalyst, N_2 adsorption/desorption isotherms (Fig. 4a) associated with the synthetized catalyst and support presents a combination of type II and type IV reference isotherms according to the IUPAC classification [37]. Type II due to the adsorption of monolayer/multilayer [38] al low P/Po. Type IV isotherm at higher partial pressures, representative of capillary condensation in presence of mesoporous [39] as evidenced by pore distribution (Fig. 4c) and pore size data collected in Table 1 and characteristic type H3 hysteresis loop. It can be observed that upon impregnation of cobalt on the support, the surface area and pore volume decreased compared to those of the parent β-SiC, demonstrating partial blockage of its pores by the metal species commented above. Note that metal incorporation did not affect the silicon carbide structure as can be seen from XRD.

N_2 adsorption/desorption isotherms of H-ZSM-5 and H-βeta zeolites (Fig. 4b) are attributed to the type I and a conjunction of types I and IV IUPAC profiles, respectively

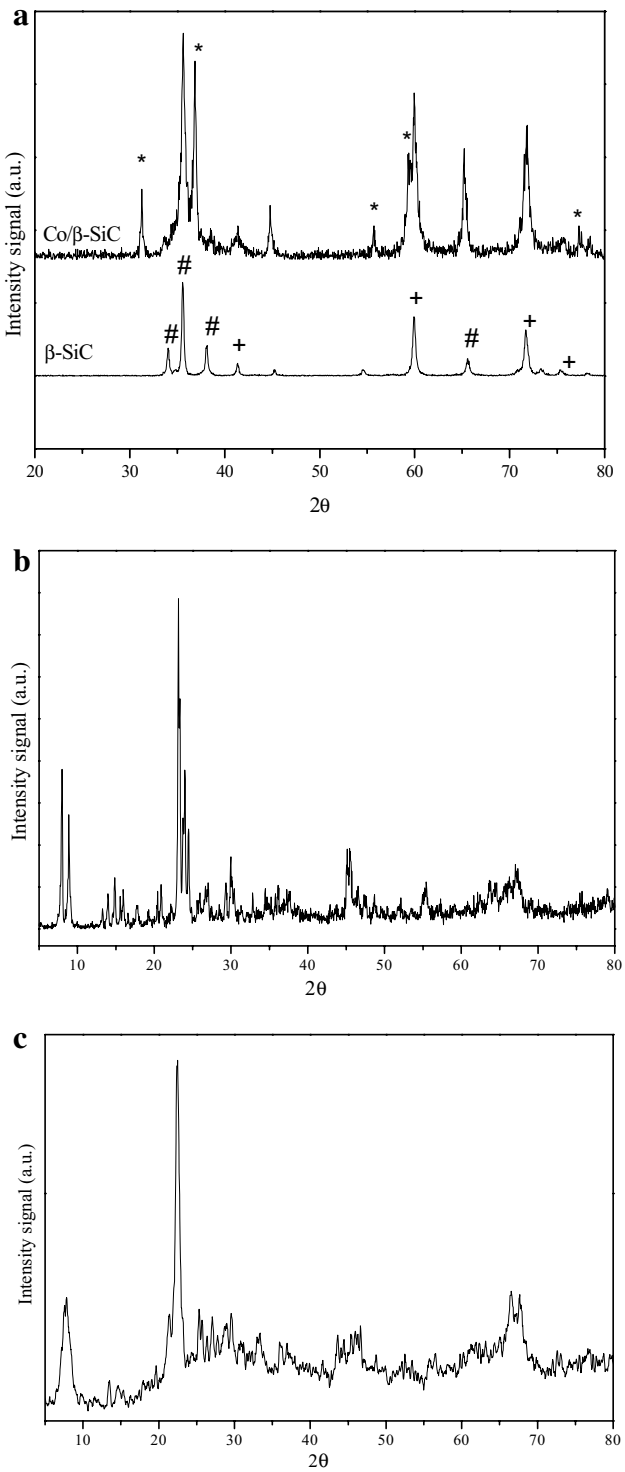

Fig. 3 XRD. **a** SiC support and catalyst Co/β-SiC, $^{+}$β-SiC, $^{\#}$α-SiC, $^{*}Co_3O_4$; **b** H-ZSM-5; **c** H-βeta

[37]. Type I isotherm is related to the presence of micropores while the H4 hysteresis loop matches that observed for a type IV isotherm and is associated to mesoporosity. Thus, once the micropores are filled at low partial pressures (P/

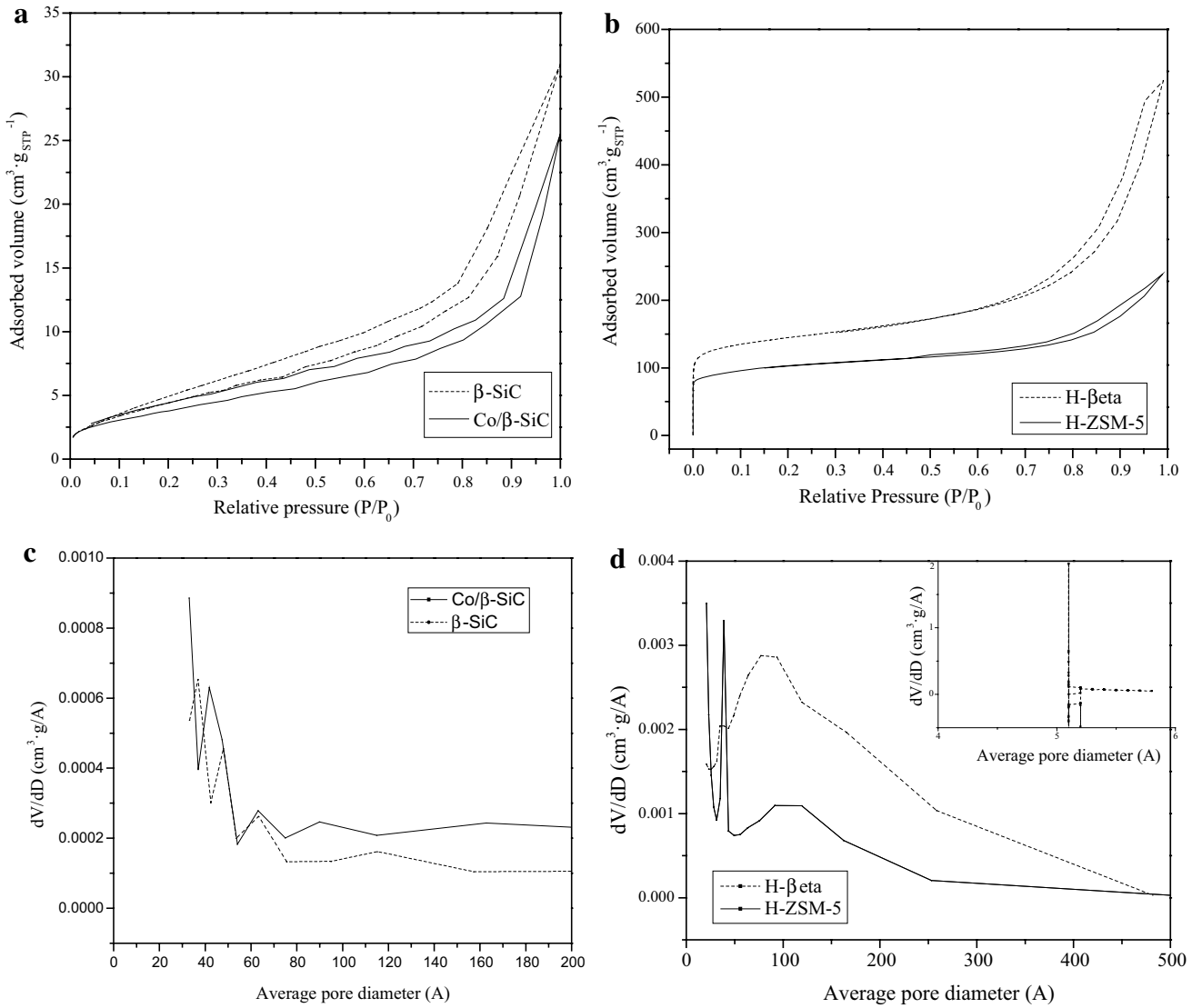

Fig. 4 N_2 adsorption/desorption isotherms of **a** Co/β-SiC and β-SiC; **b** H-ZSM-5 and H-βeta zeolites; pore size distribution of **c** Co/β-SiC and β-SiC; **d** H-ZSM-5 and H-βeta zeolites

$P_0 < 0.03$), adsorption starts in the mesopores. Note that the pronounced hysteresis loop at P/P0 > 0.4 in case of H-βeta zeolite can be due to the possible formation of nano-sized βeta crystals causing inter-particle mesoporosity as reported by Camblor and Corma [40]. In good agreement, pore volume of mesoporous in this zeolite was found to be nearly five times higher than that of microporous. Moreover, the associated pore size distribution presents expected bigger pore size for H-βeta than that of H-ZSM-5, especially in the mesoporous range (Fig. 4d), which may provide lower selectivity to gases favouring the growth of the hydrocarbon chain and, consequently, shifting C_5^+ towards high molecular weight middle distillates.

Cobalt reducibility of FTS Co/β-SiC catalyst was studied by temperature-programmed reduction analysis. As plotted in Fig. 5, two reduction peaks are clearly observed on its TPR profile. The first H_2-consumption maximum (<400 °C) can be associated with the reduction of Co_3O_4 agglomerates, the main cobalt phase obtained after calcination, to metallic phase Co^0, as reported earlier for Co/alumina catalysts [41, 42], and more specifically as α and β peaks for conventional Co/SiO_2 [43, 44] and Co*m*/SiC [45] catalyst. The second one (>700 °C) was related to the reduction of immobilized cobalt ions (silicate and hydrosilicates Co–SiO_x species with degrees of different order) [28, 46–48], which is reported to be feasible since the surface of this support seems to involve an amorphous layer of SiO_2 and SiO_xC_y species [11, 49]. In agreement with Solomonik et al. [48], it was observed that the use of subsequent impregnations with ethanol as a solvent resulted in a higher

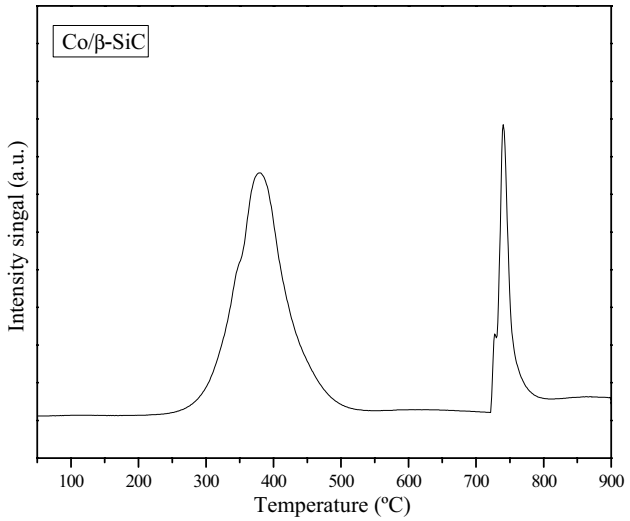

Fig. 5 TPR profile for catalyst Co/β-SiC

intensity of this high temperature maximum (compared to aqueous impregnation procedure). In addition, the percentage of reduced cobalt was analysed by pulses of oxygen (Table 1). The extent of reduction (77%) obtained for this catalyst, which is similar to those reported in the literature for Co/β-SiC catalysts [10, 45], can be attributed to a weak metal-support interaction derived from the presence of large cobalt aggregates resulting from a high cobalt loading over the low to medium specific surface area of β-SiC [28, 50].

Ammonia temperature programmed desorption profiles corresponding to the H^+-form zeolites are displayed in Fig. 6. Note that the calculated number of acid sites summarizes framework aluminum (Brönsted sites) [51] and extraframework Al– or Si–Al species possibly formed due to the post-synthesis calcination to produce the H^+-form, which can act as Lewis acid sites as described by Kombokis et al. [52]. It can be observed that zeolite H-ZSM-5 seemed to provide a higher amount of acid sites of different strength than H-βeta. Although both acid zeolites provided a wide TPD profile, zeolite H-βeta showed a maximum at lower temperature (181 °C) with a shoulder overlapped at around 300–350 °C while the profile related to zeolite H-ZSM-5 is shifted to higher desorption temperatures presenting two overlapped maxima (192 and 400 °C). The desorption peak at lower temperature (<200 °C) may be associated with NH_3 desorbed from weak silanol (Si–OH) [53, 54] although it may be also attributed to the presence of weak Lewis acidic sites [55]. Desorption peak at higher temperature (typically within 300–550 °C) can be assigned to NH_3 strongly adsorbed on acidic hydroxyl groups, i.e., Brønsted acidic sites as reported elsewhere [7, 56]. Hence, H-βeta would favour the production of higher molecular weight hydrocarbons, since the probability of chain growth is known to increase with relative basicity [57–59].

From characterization results zeolite H-βeta was expected to favour the production middle distillate hydrocarbons rather than H-ZSM-5 (gasoline) due to the combination of bigger mesopores, a higher surface area and mild acidity.

3.2 FTS Catalytic Performance

In order to study the influence of incorporating an upgrading step in a cascade mode on FTS activity and selectivity

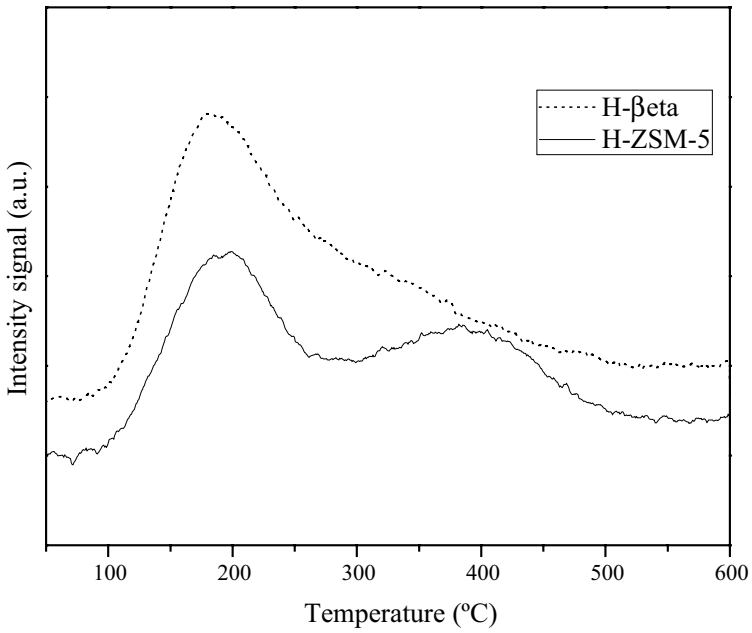

Fig. 6 NH_3-TPD profiles of H-ZSM-5 and H-βeta zeolites

over Co/β-SiC catalyst, a first series of experiments was carried out. For that purpose, a first experiment denoted as 'reference' (Co/β-SiC + inert α-SiC) was prime performed at two different reaction temperatures (220 and 250 °C). Steady state results of FTS activity, expressed in terms of FTS and WGS rates, CO and H_2 conversion, and selectivity to CO_2 and hydrocarbons are presented in Table 2. It can be observed that obtained products were mainly C_1–C_4 (mostly CH_4 although traces of ethane, ethylene, propane and propylene were also formed) and C_5^+ while CO_2 was generated in a lesser extent. At low reaction temperature and as expected from the nature of the selected Co-based catalyst, CO_2 is barely formed. Methane (10.9%) is produced in a quite lower extent than that over traditional alumina-based catalyst (up to 30%) for the same conversion level [8, 11, 60, 61]. It is well known that conventional supports such as silica or alumina provide a large specific surface area resulting in highly dispersed small cobalt crystallites. However, smaller Co particles lead to a higher concentration of hardly reducible cobalt species (aluminate or silicate-type) [42, 62, 63], which decrease catalytic activity while increasing selectivity to lower molecular weight hydrocarbons. Moreover, differences in support porosity and chemical nature also play an important role in the formation of methane. The relatively large pore size of β-SiC would allow an easy evacuation of the steam, increasing the available sites for FTS performing and consequently leading to good activity and selectivity [64, 65]. Hence, a high amount of C_5^+ is the main reaction product (82.7%), which is comparable to that obtained in previous studies over β-SiC [8, 11]. With regard to the nature of support, SiC has been proven to be chemically inert while alumina presents a certain amount of acid sites, which would prevent chain growth probability. Therefore, as reported in previous works of our group [8] and in agreement with Yu et al. [61] SiC was demonstrated to be a promising support for Co catalysts, resulting in higher reducibility and less dependence upon Co cristal size compared with conventional supports such as those commented above. Consequently, the catalytic activity of Co/β-SiC catalyst is proven to be higher while obtaining a lower selectivity to CH_4, enhancing the production of commercial hydrocarbons. However, an increase of temperature promotes CO dissociation and provides more C and H atoms that lead to the production of methane (up to 24.8% in this case). On the other hand, O atoms easily hydrogenates to H_2O favoring WGS reaction, which is demonstrated by the significant growing of CO_2 fraction up to 11%. Consequently, C_5^+ fraction considerably diminished (more than 30%) by increasing reaction temperature from 220 to 250 °C. It is important to note that H_2 conversion was higher than CO conversion in both cases in agreement with the reaction stoichiometry.

With respect to C_5^+ hydrocarbons distribution, data collected in Table 3 shows that when catalyst Co/β-SiC is used at 220 °C the major product obtained from FTS is C_{20}^+ (80 wt% waxes), which prevents production of desirable hydrocarbons such as gasoline, kerosene and diesel. By increasing reaction temperature to 250 °C the proportion of waxes was reduced up to 19 wt% since termination of growing chains due to side reactions is thermodynamically favored at those reaction conditions. Consequently, diesel, kerosene and gasoline fractions increased to 4, 27 and 50 wt% respectively.

Once the parent catalyst was checked on FTS, two blank experiments using only zeolite were run (not shown here), evincing that these materials were inert under reaction conditions and syngas feeding.

Then, in a third series of experiments, a second layer of zeolite was introduced in the reaction medium resulting in the as referred 'cascade configuration', as explained in Sect. 2.4. As reported in Table 2 and regardless the type of zeolite employed in the cascade system, FTS activity and therefore, CO conversion became more than double compared to those obtained using only Co/β-SiC due to the hydroproccesing reaction over the zeolite layer. In accordance to that reported by Egiebor et al. [66] and Martínez and López [67], since the zeolites did not show any activity for the FTS reaction under reaction conditions and syngas feeding, the increase in conversion can be associated to the cracking of waxes on the zeolite acid sites, which otherwise would gather in the FTS catalyst pores diminishing the number of active sites accessible to the reactant. It can

Table 2 FTS catalytic performance. 20 bar; $H_2/CO = 2$; GHSV = 3000 $Ncm^3\ g^{-1}\ h^{-1}$

Catalyst bed	T (°C)	Activity ($mol_{CO}\ mol_{Co}^{-1}\ h^{-1}$)		Conversion (%)		Products selectivity (%)			
		FTS	WGS	CO	H_2	CO_2	C_1	C_2–C_4	C_5^+
Co/β-SiC	220	8.2	0.1	28.7	57.4	1.2	10.9	16.1	82.7
	250	10.1	1.3	38.4	72.5	11.3	24.8	33.1	55.6
Cascade									
Co/β-SiC//H-ZSM-5	220	18.4	2.1	68.8	82.8	10.2	14.5	19.1	70.8
	250	18.6	4.8	78.9	85.6	20.9	24.9	29.9	49.1
Co/β-SiC//H-βeta	220	17.3	1.6	65.7	76.5	8.3	14.5	18.9	72.8
	250	17.6	4.1	74.6	80.2	18.9	26.7	32.4	48.6

Table 3 C_5^+ hydrocarbon product distribution. 20 bar. GHSV: 3000 $Ncm^3\ g^{-1}\ h^{-1}$. H_2/CO: 2

Catalyst bed	T (°C)	C_5^+ product selectivity (wt%)					Diesel yield (wt%)
		Gasoline (C_7–C_{10})	Kerosene (C_{11}–C_{14})	Diesel (C_{15}–C_{18})	Lubricants (C_{19}–C_{20})	Waxes (C_{20+})	
Co/β-SiC	220	10.9	8.1	1.1	0.0	79.8	0.3
	250	50.0	27.6	3.5	0.0	18.8	1.4
Cascade							
Co/β-SiC//H-ZSM-5	220	49.1	32.6	14.8	3.7	0.0	10.1
	250	63.2	25.1	10.0	1.7	0.0	7.9
Co/β-SiC//H-βeta	220	39.5	36.3	19.7	4.4	0.0	12.9
	250	55.2	32.3	12.6	0.0	0.0	9.4
Physical mixture							
Co/β-SiC + H-βeta	220	53.4	38.9	7.1	0.6	0.0	1.69
	250	59.9	31.0	7.9	1.2	0.0	5.52

be also observed that the incorporation of a zeolite layer slightly modified the selectivity to methane, which demonstrated that methane formation is mainly caused by the FTS function determined by the proposed Co/β-SiC catalyst. It also evinced that no overcracking was seemed to occur at the low temperatures employed in the present work, since methane is supposed to be formed by protolytic cracking on the zeolite acid sites at temperatures higher than 450 °C [54, 55]. However, the activity of the WGS secondary reaction was increase under cascade configuration, where zeolites were present. CO_2 formation was 8–10 times higher at lower reaction temperature although this effect was seemed to be quietly reduced when increasing reaction temperature. Accordingly, this fact could be attributed to the favored steam condensation by trapping in the condensed liquid. Therefore, although selectivity to C_5^+ hydrocarbon was slightly diminished (7–10%), the yield to C_7–C_{18} and, particularly diesel, was increased. However, it should be note that the most remarkable influence of this configuration

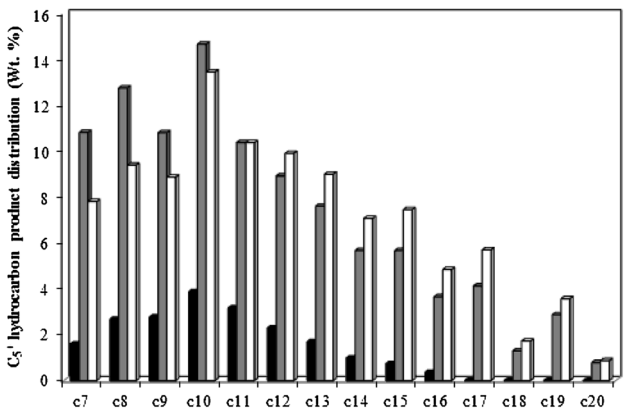

Fig. 7 Influence of cascade system on C_5^+ hydrocarbon product distribution. Reaction conditions: 20 bar. 220 °C. GHSV: 3000 $Ncm^3\ g^{-1}\ h^{-1}$. H_2/CO: 2. *Black filled square* Co/β-SiC, *gray filled square* Co/β-SiC/H-ZSM-5, *unfilled square* Co/β-SiC/H-βeta

system was the shift of heavy hydrocarbons to middle distillate, completely varying C_5^+ product distribution. As exposed in Table 3, no waxes were collected due to zeolite hydrocracking under the proposed cascade configuration, while liquid hydrocarbons were displaced towards C_7–C_{18} fractions and, in a lesser extent, to C_{19}–C_{20}. It is worth mentioning that the present results improved those obtained by incorporating a zeolite to catalyst Co/SiO_2 [68] where the complete removal of waxes was not possible. Furthermore, catalytic results showed that, as expected, the nature of the zeolite modified the selectivity to C_5^+ hydrocarbons. At the same reaction conditions, H-ZSM-5 shifted hydrocarbon distribution to mainly gasoline fraction, while zeolite H-βeta, despite the high production of gasoline, promoted the production of middle distillates, specifically enhancing kerosene and diesel distillates (Fig. 7). According to literature and characterization results, this difference is due to the mild acidity and higher pore size of zeolite H-βeta. Particularly, its larger pore diameter and pore volume facilitate diffusion of large molecule reactants and the production of longer chain hydrocarbons [52].

Although further research is needed, in view of these results, the feasibility of the proposed configuration for the integration of FTS and hydrocracking in a single unit was demonstrated. However, considering that the ultimate goal of this research is the complete elimination of waxes while promoting middle distillates production, among both zeolites, zeolite H-βeta was found to be more suitable to that end than H-ZSM-5.

Finally, in order to verify the effectiveness of the cascade system, the physical mixture of Co/β-SiC and zeolite H-βeta was tested. As shown in Fig. 8, it can be observed that although a higher hydrocracking activity of the physical mixture should be expected, at low reaction temperature CO conversion obtained under this configuration was even lower than that using just the FTS catalyst. It could be attributed to diffusion limitations due to the higher amount

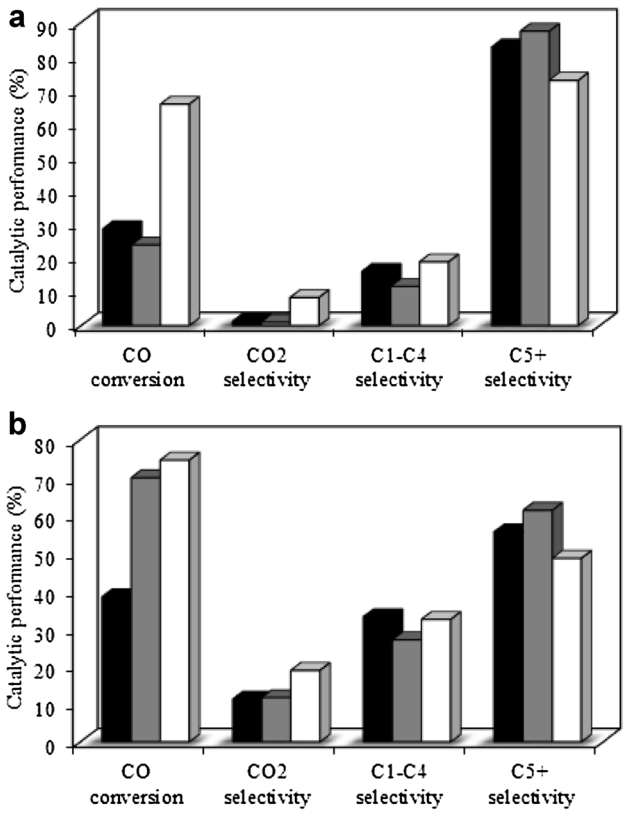

Fig. 8 Influence of configuration system on FTS catalytic performance. Reaction conditions: 20 bar. GHSV: 3000 $Ncm^3\ g^{-1}\ h^{-1}$. H_2/CO: 2. **a** 220 °C; **b** 250 °C. *Black filled square* Co/β-SiC, *gray filled square* Co/β-SiC + H-βeta, *unfilled square* Co/β-SiC//H-βeta

of waxes in the medium, which may cover acid active sites in the zeolite. The wax restrains water from the catalyst, preventing the adsorption on the acidic sites of the zeolite. In agreement, once temperature was raised leading to an increased hydrocracking and hence, a lower amount of waxes was produced, CO conversion was found to increase. It can be also due to an hydrodynamical effect as reported by Botes and Böhringer over Fe and H-ZSM-5 performed in a Berty reactor [69]. However, it should be note that the high reaction temperature required for an effective performance under physical mixture configuration may result in the deactivation of the catalyst by coke deposition [17].

Regarding C_5^+ hydrocarbon product distribution, as shown in Table 3, it is to be emphasized that regardless of the position of the zeolite in the catalyst configuration, the wax fraction completely disappeared and liquid hydrocarbons were displaced towards C_7–C_{18} fractions and, in a lesser extent, to C_{19}–C_{20}. Results summarized in that Table also indicates that with no dependence on the reaction temperature, the use of a cascade catalyst system resulted in a higher production of synthetic diesel than that when using a physical mixture. The closer vicinity of acid sites and FTS function in the physical mixture has been reported to promote overcracking [70] to gasoline, as demonstrated in Table 3.

Taking into account that above, the proposed cascade system was confirmed to be a suitable alternative for the direct production of middle distillates.

4 Conclusions

This article examines the effect of integrated upgrading on FTS products in a cascade-bed reactor system, which allows FTS and cracking stages to occur sequentially. Composed of two sequential catalyst layers, the proposed cascade system was found to remedy the main problem related to conventional stand-alone catalyst configuration. Fischer–Tropsch synthesis with good activity and C_{5+} selectivity was demonstrated on a Co-based catalyst supported on β-SiC carrier. Moreover, the utilization of a subsequent layer of H-ZSM-5 or H-βeta (acid zeolites with different framework topologies) was active for cracking heavy FT products into C_7–C_{18}. H-βeta zeolite, which presents a mild acidity and larger pore size, lead to suppress the overcracking of heavy hydrocarbons resulting in a significant improvement of middle distillates production than H-ZSM-5. Different to prior studies, the completely elimination of waxes was achieved along with an enhancement of not only gasoline but also kerosene and diesel yields. Compared to the physical mixture, the proposed cascade configuration was demonstrated to enhance the production of commercial fuels, especially at low reaction temperature. Therefore, Co/β-SiC//H-βeta system is effective in the selective synthesis of the middle distillates-ranged hydrocarbons from syngas.

Acknowledgements Sicat catalyst is gratefully acknowledged for providing support sample.

References

1. Leckel D (2009) Diesel production from Fischer–Tropsch: the past, the present, and new concepts. Energy Fuels 23(5):2342–2358. doi:10.1021/ef900064c
2. Wang Y (2011) Development of highly selective Fischer–Tropsch catalysts for production of diesel- and gasoline-range hydrocarbons. In: ACS National Meeting Book of Abstracts
3. Liu G, Larson ED, Williams RH, Kreutz TG, Guo X (2011) Making Fischer–Tropsch fuels and electricity from coal and biomass: performance and cost analysis. Energy Fuels 25(1):415–437. doi:10.1021/ef101184e
4. Sartipi S, Makkee M, Kapteijn F, Gascon J (2014) Catalysis engineering of bifunctional solids for the one-step synthesis of liquid fuels from syngas: a review. Catal Sci Technol 4(4):893–907. doi:10.1039/c3cy01021j

5. Freitez A, Pabst K, Kraushaar-Czarnetzki B, Schaub G (2011) Single-stage Fischer–Tropsch synthesis and hydroprocessing: the hydroprocessing performance of Ni/ZSM-5/γ-Al_2O_3 under Fischer–Tropsch conditions. Ind Eng Chem Res 50(24):13732–13741. doi:10.1021/ie201913s
6. Sun B, Yu G, Lin J, Xu K, Pei Y, Yan S, Qiao M, Fan K, Zhang X, Zong B (2012) A highly selective Raney Fe@HZSM-5 Fischer–Tropsch synthesis catalyst for gasoline production: one-pot synthesis and unexpected effect of zeolites. Catal Sci Technol 2(8):1625–1629. doi:10.1039/c2cy20155k
7. Cheng K, Kang J, Huang S, You Z, Zhang Q, Ding J, Hua W, Lou Y, Deng W, Wang Y (2012) Mesoporous beta zeolite-supported ruthenium nanoparticles for selective conversion of synthesis gas to C_5–C_{11} isoparaffins. ACS Catal 2(3):441–449. doi:10.1021/cs200670j
8. de la Osa AR, de Lucas A, Sánchez-Silva L, Díaz-Maroto J, Valverde JL, Sánchez P (2012) Performing the best composition of supported Co/SiC catalyst for selective FTS diesel production. Fuel 95(0):587–598. doi:10.1016/j.fuel.2011.11.002
9. de Tymowski B, Liu Y, Meny C, Lefèvre C, Begin D, Nguyen P, Pham C, Edouard D, Luck F, Pham-Huu C (2012) Co–Ru/SiC impregnated with ethanol as an effective catalyst for the Fischer–Tropsch synthesis. Appl Catal A 419–420(0):31–40. doi:10.1016/j.apcata.2012.01.004
10. Díaz JA, Calvo-Serrano M, de la Osa AR, García-Minguillán AM, Romero A, Giroir-Fendler A, Valverde JL (2014) β-silicon carbide as a catalyst support in the Fischer–Tropsch synthesis: Influence of the modification of the support by a pore agent and acidic treatment. Appl Catal A 475(0):82–89. doi:10.1016/j.apcata.2014.01.021
11. Lacroix M, Dreibine L, de Tymowski B, Vigneron F, Edouard D, Bégin D, Nguyen P, Pham C, Savin-Poncet S, Luck F, Ledoux M-J, Pham-Huu C (2011) Silicon carbide foam composite containing cobalt as a highly selective and re-usable Fischer–Tropsch synthesis catalyst. Appl Catal A 397(1–2):62–72. doi:10.1016/j.apcata.2011.02.012
12. Ledoux MJ, Pham-Huu C (2001) Silicon carbide a novel catalyst support for heterogeneous catalysis. CATTECH 5(4):226–246. doi:10.1023/a:1014092930183
13. Lee JS, Jung JS, Moon DJ (2015) The Effect of cobalt loading on Fischer Tropsch synthesis over silicon carbide supported catalyst. J Nanosci Nanotechnol 15(1):396–399. doi:10.1166/jnn.2015.8350
14. Lillebø A, Håvik S, Blekkan EA, Holmen A (2013) Fischer–Tropsch synthesis on SiC-supported cobalt catalysts. Top Catal 56(9–10):730–736. doi:10.1007/s11244-013-0032-3
15. Zhang Q, Kang J, Wang Y (2010) Development of novel catalysts for Fischer–Tropsch synthesis: tuning the product selectivity. ChemCatChem 2(9):1030–1058. doi:10.1002/cctc.201000071
16. Ge Q, Li X, Kaneko H, Fujimoto K (2007) Direct synthesis of LPG from synthesis gas over Pd–Zn–Cr/Pd-β hybrid catalysts. J Mol Catal A 278(1–2):215–219. doi:10.1016/j.molcata.2007.09.008
17. Martínez A, Rollán J, Arribas MA, Cerqueira HS, Costa AF, S.-Aguiar EF (2007) A detailed study of the activity and deactivation of zeolites in hybrid Co/SiO_2-zeolite Fischer–Tropsch catalysts. J Catal 249(2):162–173. doi:10.1016/j.jcat.2007.04.012
18. Zhang S, Xu R, Durham E, Roberts CB (2014) Middle distillates production via Fischer–Tropsch synthesis with integrated upgrading under supercritical conditions. AlChE J 60(7):2573–2583. doi:10.1002/aic.14493
19. Pabst K, Kraushaar-Czarnetzki B, Schaub G (2013) Combination of Fischer–Tropsch synthesis and hydroprocessing in a single-stage reactor. Part II. Effect of catalyst combinations. Ind Eng= Chem Res 52(26):8988–8995. doi:10.1021/ie3030483
20. de la Osa AR, De Lucas A, Díaz-Maroto J, Romero A, Valverde JL, Sánchez P (2012) FTS fuels production over different Co/SiC catalysts. Catal Today 187(1):173–182. doi:10.1016/j.cattod.2011.12.029
21. Ma T, Imai H, Shige T, Sugio T, Li X (2015) Synthesis of hydrocarbons from H_2-deficient syngas in Fischer–Tropsch synthesis over co-based catalyst coupled with fe-based catalyst as water-gas shift reaction. J Nanomater 2015:10. doi:10.1155/2015/268121
22. Ma T, Imai H, Yamawaki M, Terasaka K, Li X (2014) Selective synthesis of gasoline-ranged hydrocarbons from syngas over hybrid catalyst consisting of metal-loaded ZSM-5 coupled with copper-zinc oxide. Catalysts 4(2):116
23. Brunauer S, Emmett PH, Teller E (1938) Adsorption of gases in multimolecular layers. J Am Chem Soc 60(2):309–319
24. Barrett EP, Joyner LG, Halenda PP (1951) The determination of pore volume and area distributions in porous substances. I. Computations from nitrogen isotherms. J Am Chem Soc 73(1):373–380
25. Cheng LS, Ralph TY (1994) Improved Horvath-Kawazoe equations including spherical pore models for calculating micropore size distribution. Chem Eng Sci 49(16):2599–2609. doi:10.1016/0009-2509(94)E0054-T
26. Hilmen AM, Schanke D, Hanssen KF, Holmen A (1999) Study of the effect of water on alumina supported cobalt Fischer–Tropsch catalysts. Appl Catal A 186(1–2):169–188. doi:10.1016/S0926-860X(99)00171-4
27. Scherrer P (1918). Nachrichten von der Gesellschaft der Wissenschaften zu Göttingen 2:98
28. Jacobs G, Das TK, Zhang Y, Li J, Racoillet G, Davis BH (2002) Fischer–Tropsch synthesis: support, loading, and promoter effects on the reducibility of cobalt catalysts. Appl Catal A 233(1–2):263–281. doi:10.1016/S0926-860X(02)00195-3
29. Storsæter S, Tøtdal B, Walmsley JC, Tanem BS, Holmen A (2005) Characterization of alumina-, silica-, and titania-supported cobalt Fischer–Tropsch catalysts. J Catal 236(1):139–152. doi:10.1016/j.jcat.2005.09.021
30. Yuan X, Lü J, Yan X, Hu L, Xue Q (2011) Preparation of ordered mesoporous silicon carbide monoliths via preceramic polymer nanocasting. Microporous Mesoporous Mater 142(2–3):754–758. doi:10.1016/j.micromeso.2011.01.014
31. Jacobson NS, Myers DL (2011) Active oxidation of SiC. Oxid Met 75(1–2):1–25. doi:10.1007/s11085-010-9216-4
32. Lee S-H, Yun S-M, Kim S, Park S-J, Lee Y-S (2010) Characterization of nanoporous β-SiC fiber complex prepared by electrospinning and carbothermal reduction. Res Chem Intermed 36(6–7):731–742. doi:10.1007/s11164-010-0175-9
33. Ledoux MJ, Crouzet C, Pham-Huu C, Turines V, Kourtakis K, Mills PL, Lerou JJ (2001) High-yield butane to maleic anhydride direct oxidation on vanadyl pyrophosphate supported on heat-conductive materials: β-SiC, Si3N4, and BN. J Catal 203(2):495–508. doi:10.1006/jcat.2001.3344
34. Rane S, Borg Ø, Yang J, Rytter E, Holmen A (2010) Effect of alumina phases on hydrocarbon selectivity in Fischer–Tropsch synthesis. Appl Catal A 388(1–2):160–167. doi:10.1016/j.apcata.2010.08.038
35. Triantafyllidis KS, Nalbandian L, Trikalitis PN, Ladavos AK, Mavromoustakos T, Nicolaides CP (2004) Structural, compositional and acidic characteristics of nanosized amorphous or partially crystalline ZSM-5 zeolite-based materials. Microporous Mesoporous Mater 75(1–2):89–100. doi:10.1016/j.micromeso.2004.07.016
36. Mavrodinova VP (1998) Solid-state ion exchange in beta zeolites. I: alkaline chlorides/NH_4-β. Microporous Mesoporous Mater 24(1–3):1–8. doi:10.1016/S1387-1811(98)00138-3
37. Rouquerol J, Avnir D, Everett DH, Fairbridge C, Haynes M, Pernicone N, Ramsay JDF, Sing KSW, Unger KK (1994) Guidelines

for the characterization of porous solids. In: Rouquerol FR-RKSWS J, Unger KK (eds) Studies in surface science and catalysis, vol 87. Elsevier, Amsterdam, pp 1–9. doi:10.1016/S0167-2991(08)63059-1
38. Kolasinski KW (ed) (2007) Surface science foundations of catalysis and nanoscience. Wiley, Chichester
39. Sing KSW, Everett DH, Haul RAW, Moscou L, Pierotti RA, Rouquerol J (1985) Pure Appl Chem 57:16
40. Camblor MA, Corma A, Valencia S (1998) Characterization of nanocrystalline zeolite Beta. Microporous Mesoporous Mater 25(1–3):59–74. doi:10.1016/S1387-1811(98)00172-3
41. Arnoldy P, Moulijn JA (1985) Temperature-programmed reduction of $CoOAI_2O_3$ catalysts. J Catal 93(1):38–54. doi:10.1016/0021-9517(85)90149-6
42. Bechara R, Balloy D, Dauphin J-Y, Grimblot J (1999) Influence of the characteristics of γ-aluminas on the dispersion and the reducibility of supported cobalt catalysts. Chem Mater 11(7):1703–1711. doi:10.1021/cm981015n
43. Schanke D, Vada S, Blekkan EA, Hilmen AM, Hoff A, Holmen A (1995) Study of Pt-promoted cobalt CO hydrogenation catalysts. J Catal 156(1):85–95. doi:10.1006/jcat.1995.1234
44. Rodrigues EL, Bueno JMC (2002) Co/SiO_2 catalysts for selective hydrogenation of crotonaldehyde II: Influence of the Co surface structure on selectivity. Appl Catal A 232(1–2):147–158. doi:10.1016/s0926-860x(02)00090-x
45. de la Osa A, Romero A, Dorado F, Valverde J, Sánchez P (2016) Influence of cobalt precursor on efficient production of commercial fuels over FTS Co/SiC Catalyst. Catalysts 6(7):98
46. Batista MS, Santos RKS, Assaf EM, Assaf JM, Ticianelli EA (2004) High efficiency steam reforming of ethanol by cobalt-based catalysts. J Power Sources 134(1):27–32. doi:10.1016/j.jpowsour.2004.01.052
47. Zhou W, Chen J-G, Fang K-G, Sun Y-H (2006) The deactivation of Co/SiO_2 catalyst for Fischer–Tropsch synthesis at different ratios of H_2 to CO. Fuel Process Technol 87 (7):609–616. doi:10.1016/j.fuproc.2006.01.008
48. Solomonik IG, Gryaznov KO, Skok VF, Mordkovich VZ (2015) Formation of surface cobalt structures in SiC-supported Fischer–Tropsch catalysts. RSC Adv 5(96):78586–78597. doi:10.1039/c5ra11853k
49. Nguyen P, Pham C (2011) Innovative porous SiC-based materials: from nanoscopic understandings to tunable carriers serving catalytic needs. Appl Catal A 391(1–2):443–454. doi:10.1016/j.apcata.2010.07.054
50. Xiong H, Zhang Y, Liew K, Li J (2008) Fischer–Tropsch synthesis: the role of pore size for Co/SBA-15 catalysts. J Mol Catal A 295(1–2):68–76. doi:10.1016/j.molcata.2008.08.017
51. Parrillo DJ, Lee C, Gorte RJ (1994) Heats of adsorption for ammonia and pyridine in H-ZSM-5: evidence for identical Brønsted-acid sites. Appl Catal A 110(1):67–74. doi:10.1016/0926-860X(94)80106-1
52. Komvokis VG, Karakoulia S, Iliopoulou EF, Papapetrou MC, Vasalos IA, Lappas AA, Triantafyllidis KS (2012) Upgrading of Fischer–Tropsch synthesis bio-waxes via catalytic cracking: Effect of acidity, porosity and metal modification of zeolitic and mesoporous aluminosilicate catalysts. Catal Today 196(1):42–55. doi:10.1016/j.cattod.2012.06.029
53. Gorte RJ (1999) What do we know about the acidity of solid acids?. Catal Lett 62(1):1–13
54. Putluru SSR, Riisager A, Fehrmann R (2011) Alkali resistant Cu/zeolite $deNO_x$ catalysts for fuel gas cleaning in biomass fired applications. Appl Catal B 101(3–4):183–188. doi:10.1016/j.apcatb.2010.09.015
55. Akah AC, Nkeng G, Garforth AA (2007) The role of Al and strong acidity in the selective catalytic oxidation of NH3 over Fe-ZSM-5. Appl Catal B 74(1–2):34–39. doi:10.1016/j.apcatb.2007.01.009
56. Hidalgo CV, Itoh H, Hattori T, Niwa M, Murakami Y (1984) Measurement of the acidity of various zeolites by temperature-programmed desorption of ammonia. J Catal 85(2):362–369. doi:10.1016/0021-9517(84)90225-2
57. Bao A, Liew K, Li J (2009) Fischer–Tropsch synthesis on CaO-promoted Co/Al_2O_3 catalysts. J Mol Catal A 304(1–2):47–51. doi:10.1016/j.molcata.2009.01.022
58. de la Osa AR, De Lucas A, Valverde JL, Romero A, Monteagudo I, Coca P, Sánchez P (2011) Influence of alkali promoters on synthetic diesel production over Co catalyst. Catal Today 167(1):96–106. doi:10.1016/j.cattod.2010.11.064
59. Dry ME, Oosthuizen GJ (1968) The correlation between catalyst surface basicity and hydrocarbon selectivity in the Fischer–Tropsch synthesis. J Catal 11(1):18–24. doi:10.1016/0021-9517(68)90004-3
60. de la Osa AR, De Lucas A, Romero A, Valverde JL, Sánchez P (2011) Influence of the catalytic support on the industrial Fischer–Tropsch synthetic diesel production. Catal Today 176(1):298–302. doi:10.1016/j.cattod.2010.12.010
61. Yu L, Liu X, Fang Y, Wang C, Sun Y (2013) Highly active Co/SiC catalysts with controllable dispersion and reducibility for Fischer–Tropsch synthesis. Fuel 112(0):483–488. doi:10.1016/j.fuel.2013.04.072
62. Ernst B, Bensaddik A, Hilaire L, Chaumette P, Kiennemann A (1998) Study on a cobalt silica catalyst during reduction and Fischer–Tropsch reaction: In situ EXAFS compared to XPS and XRD. Catal Today 39(4):329–341. doi:10.1016/S0920-5861(97)00124-7
63. Khodakov AY, Lynch J, Bazin D, Rebours B, Zanier N, Moisson B, Chaumette P (1997) Reducibility of cobalt species in silica-supported Fischer–Tropsch catalysts. J Catal 168(1):16–25. doi:10.1006/jcat.1997.1573
64. Ghampson IT, Newman C, Kong L, Pier E, Hurley KD, Pollock RA, Walsh BR, Goundie B, Wright J, Wheeler MC, Meulenberg RW, Desisto WJ, Frederick BG, Austin RN (2010) Effects of pore diameter on particle size, phase, and turnover frequency in mesoporous silica supported cobalt Fischer–Tropsch catalysts. Appl Catal A 388(1–2):57–67. doi:10.1016/j.apcata.2010.08.028
65. Song D, Li J (2006) Effect of catalyst pore size on the catalytic performance of silica supported cobalt Fischer–Tropsch catalysts. J Mol Catal A 247(1–2):206–212. doi:10.1016/j.molcata.2005.11.021
66. Egiebor NO, Cooper WC, Wojciechowski BW (1989) Synthesis of motor fuels from HY-zeolite supported Fischer–Tropsch iron catalysts. Appl Catal 55 (1):47–64. doi:10.1016/S0166-9834(00)82316-7
67. Martínez A, López C (2005) The influence of ZSM-5 zeolite composition and crystal size on the in situ conversion of Fischer–Tropsch products over hybrid catalysts. Appl Catal A 294(2):251–259. doi:10.1016/j.apcata.2005.07.038
68. Karre AV, Kababji A, Kugler EL, Dadyburjor DB (2013) Effect of time on stream and temperature on upgraded products from Fischer–Tropsch synthesis when zeolite is added to iron-based activated-carbon-supported catalyst. Catal Today 214:82–89. doi:10.1016/j.cattod.2013.04.010
69. Botes FG, Böhringer W (2004) The addition of HZSM-5 to the Fischer–Tropsch process for improved gasoline production. Appl Catal A 267(1–2):217–225. doi:10.1016/j.apcata.2004.03.006
70. Oukaci R, Wu JCS, Goodwin JG (1988) Effect of SiAl ratio on secondary reactions during CO hydrogenation on zeolite-supported metal catalysts. J Catal 110(1):47–57. doi:10.1016/0021-9517(88)90296-5